Physical origin of pressure- and saturation fluctuations in steady-state core floods

Steffen Berg[1,*], *Hilbert* van der Linde[1], *Niels* Brussee[1], *Maja* Rücker[2,3], *Harm* Dijk[4], *Evren* Unsal[1], *Tibi G.* Sorop[1], and *Matthias* Appel[1]

[1]Shell Global Solutions International B.V., Grasweg 31, 1031 HW Amsterdam, The Netherlands
[2]Department of Mechanical Engineering, Technical University Eindhoven, De Rondom 70, 5612 AP Eindhoven, The Netherlands
[3]Department of Chemical Engineering Imperial College London, United Kingdom
[4]Shell Global Solutions International B.V., Lange Kleiweg 40, Rijswijk, 2288 GK, Netherlands

Abstract. Relative permeability is traditionally obtained in core flooding experiments during which water and oil phases are co-injected, using either using simplified analytical methods or by inverse modelling (history matching) including assisted/automated methods. However, in many steady-state (fractional flow) core flooding experiments significant fluctuations in pressure and saturation are observed, which can lead to increased uncertainty ranges of relative permeability and may even persuade experimentalists to dismiss the experiment altogether. Here we provide a more detailed insight into fluctuations and show that they may not always be related to instrumental artefacts such as produced by back pressure regulators, but rather have a physical origin. Over the past decade we have learned that pore scale displacement events such as Haines jumps and snap-off can lead to small pressure pulses. Moreover, recent synchrotron-beamline based fast micro-CT experiments clearly show that collective displacements on a millimeter-sized scale of the oil cluster may lead to pressure- and saturation fluctuations on similar magnitude as typically observed in classical SCAL steady-state experiments on samples of several centimeters length and diameter. Furthermore, when monitoring pressure and saturation on a centimeter length scale we sometimes observe, depending on wettability and other parameters, periodic fluctuations which are accompanied by travelling waves in the saturation profiles. While the origin of such fluctuations are likely pore-scale events one would expect that on a Darcy-scale, such fluctuations of pore scale origin would average and decay very quickly. However, a more detailed analysis shows that such Darcy-scale solutions for traveling waves leading to fluctuations in pressure and saturation are permissible by fractional flow theory. The adequate interpretation of such phenomena requires consideration of both drainage and imbibition relative permeability bounding curves and respective hysteresis models. A potential physical reason is that travelling waves can have higher total mobility than a flat saturation profile.

1 Introduction

For most subsurface applications such as dynamic modelling in reservoir engineering, multiphase flow in porous rock is described with the multiphase extension of Darcy's law. That is a continuum formulation where the phase fluxes are linearly related to the respective pressure gradients. While very effective from a practical perspective, one of the consequences of this phenomenological extension is that the flow parameters such as relative permeability and capillary pressure need to be determined experimentally or more recently with Digital Rock methods. Relative permeability is typically determined in core flooding experiments where in particular the steady-state method is preferred because of a number of reasons [1, 2]. As illustrated in Figure 1, in steady-state core flooding experiments the relative permeability is determined from the average pressure-drop at the end of each fractional flow step.

However, in many steady-state experiments, depending on a range of factors, sometimes very "large" pressure fluctuations are observed [3-7] which can be significantly larger than instrumental noise e.g. from pressure transducers.

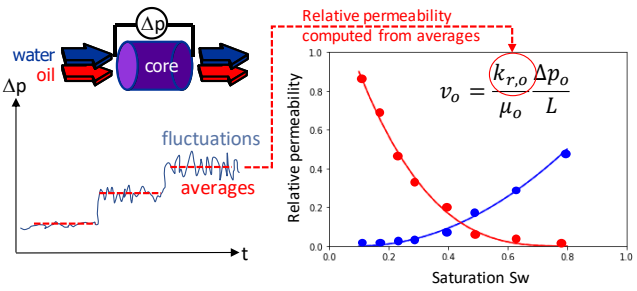

Figure 1. Steady-state core flooding experiments: water and oil phases are co-injected at varying fractional flow f_w. Relative permeability is determined from the average pressure drops at each f_w while the raw data often shows sometimes significant fluctuations in pressure drop and saturation.

In the past, in special core analysis (SCAL) programs large fluctuations in pressure drop or saturation [3-11] have been

* Corresponding author: steffen.berg@shell.com

interpreted as experimental artefacts as they can be potentially also caused by e.g. back pressure regulators, which has led in many cases to the dismissal of the data set. Pressure fluctuations have been also observed in many pore-scale experiments [8-24]. In [9] the connection between pressure and saturation fluctuations in Darcy-scale experiments and pore scale displacement events and respective flow regimes such as ganglion dynamics [25-27] and intermittency [14-18] has been made. Individual pore filling events and associated capillary fluctuations are expected to average out at the Darcy scale (i.e. when averaged over hundreds to thousands of pores) at least for stationary processes and not lead to a significant saturation. However, that is not what is experimentally observed [3-11]. In a range of independent experiments, with different setups, by different groups, significant saturation fluctuations were observed which exceed the level of individual pore filling events by orders of magnitude. That raises the question about the underlying cause of pressure and saturation fluctuations at the Darcy scale, i.e. whether they reflect the movement of large oil clusters in a ganglion dynamics flow regime [26, 27], or if there is actually another reason why we sometimes observe significant pressure fluctuations.

In this work we address this question by analyzing a steady-state fractional flow experiment in significantly more detail than normally done in the interpretation of steady-state experiments. The experiment has been designed to suppress all known experimental artefacts that could cause fluctuations i.e. no back-pressure controller is involved but fluids are re-circulated, pulse-free injection pumps with zero-dead volume switching pumps are used and monitored for continuous injection, the fluid pair chosen cannot form emulsions, etc.

We show that large pressure and saturation fluctuations are associated with travelling saturation waves consisting of sequences of drainage and imbibition. The main conclusion is that Darcy scale saturation fluctuations can be reconciled with fractional flow solutions for a hysteretic drainage and imbibition relative permeability pair.

There are several consequences for the interpretation and application of relative permeability observed from such an experiment ranging from the insight that e.g. drainage relative permeability may involve elements of imbibition and vice versa and obtained relative permeability is in fact on a scanning curve. There are also potential consequences whether in presence of significant fluctuations the 2-phase Darcy equations correctly represent the dissipation of energy.

2 Methods and Materials

2.1 Flow experiment

Steady-state core flooding experiments are performed in an experimental setup illustrated in **Figure 2** which is similar to the ones used routinely for relative permeability SCAL measurements [28,3,4]. Water and oil phases are co-injected with pulse-free Quizzix pumps (Chandler, Metek) equipped with with zero-dead volume switching valves for smooth and pulse-free continuous flow (Vindum Engineering) at fractional flow

$$f_w = \frac{q_w}{q_w + q_o} \qquad (1)$$

where q_w and q_o are the volumetric rate of water and oil phase, respectively.

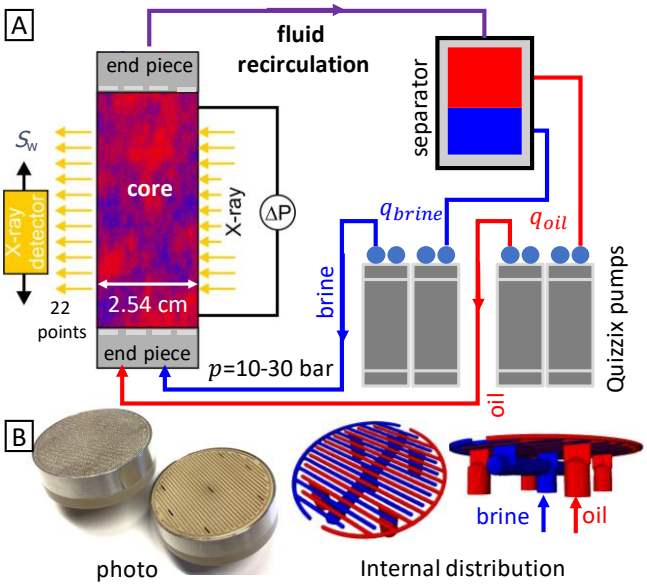

Figure 2. (A) Steady-state core flooding experimental setup where water and oil phases are co-injected at varying fractional flow f_w with 2 dual-piston Quizzix pumps that operate with zero-dead volume switching valves for smooth and pulse-free continuous flow. Typically, fluids are re-circulated (after separation) without any back-pressure controller to accommodate for large number of injected pore volumes. Saturation is monitored in-situ with a linear X-ray system. (B) Photo of the end piece (with and without the metal mesh) and internal distribution network providing a continuous injection of oil and brine across the end face of the core.

Water saturation S_w is determined by in-situ X-ray monitoring using a linear X-ray scanner at 22 positions along the core (using an X-ray transparent core holder) at time intervals of 8 min 30s. Saturation from X-ray was consistent with an Amott spontaneous imbibition test. Electrical conductivity along the core is recorded at the same time interval. Pressure drop Δp along the core and the central section, outside of capillary end-effects [29], is monitored at a time interval of 1 min. The flow rate is kept constant at $q_w + q_o = 3\ ml/min$ corresponding to a capillary number of 10^{-5} which is still below the onset of capillary de-saturation. More details are give in [30,28].

Experiments started with primary drainage at $S_w = 1$ injecting at $f_w = 1.0$ (brine only) which is stepwise reduced to $f_w = 0.0$ (oil only), followed by imbibition starting at $f_w = 0.0$ which is systematically increased to $f_w = 1.0$. At each f_w step pressure-drop Δp, saturation S_w and electrical conductivity are monitored. The steady state is experimentally achieved when Δp and S_w are stable (vary by less than 1%) and relative permeability $k_{r,\alpha}$ is then computed (at each f_w) using the two-phase Darcy equation

$$q_\alpha = -\frac{k_{r,\alpha}}{\mu_\alpha} AK \frac{\Delta p_\alpha}{L} \qquad (2)$$

where K is the (absolute) permeability of the rock, L the length and A the cross-sectional area of the cylindrical rock sample, μ_α the viscosity of phase $\alpha = o, w$ (oil, water).

2.2 Rock, Fluids

A cylindrical sample of Fontainebleau sandstone [31,32] with diameter d=2.54 cm and length L=4.45 cm was used. It has a porosity of ϕ=0.13 and permeability K=539 mD. Prior to the experiment the sample was cleaned by Soxhlet extraction (chloroform-methanol) The sample remained strongly water-wet after the Soxhlet extraction. The fluids were n-decane with a density of 731.9 kg/m^3 and a viscosity of 0.933 mPas, and NaCl brine doped with 5% CsCl, with a density of 1037 kg/m^3 and viscosity of 0.992 mPas. The interfacial tension was approximately 40 mN/m.

3 Results

3.1 Raw data of fractional flow experiments

In **Figure 3** the pressure drop Δp of a primary drainage experiment conducted on the Fontainebleau sandstone rock is displayed for the first two cycles (out of 5). The sample had been cleaned in-between with isopropanol inside the core holder without removing the sample. Both experiments show in a repeatable way a lesser degree of fluctuations at high fractional flows and the end of drainage while at intermediate fractional flows between $0.75 \geq f_w \geq 0.1$ significant pressure fluctuations are observed. The imbibition data and further cycles (not shown) reproduce the pattern in a conceptually similar manner.

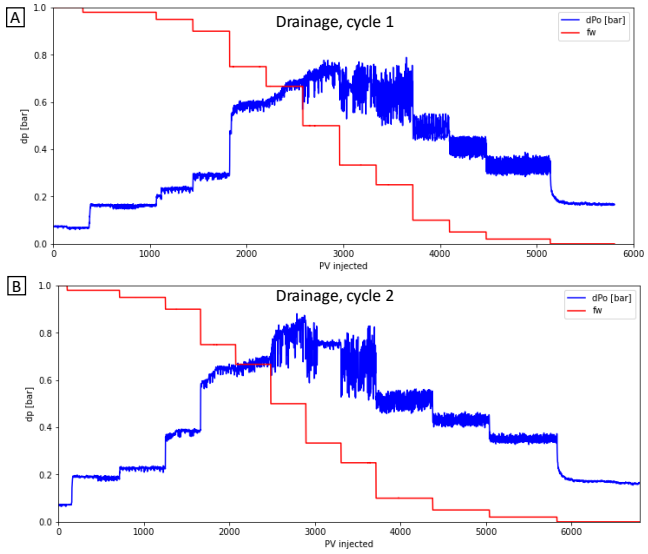

Figure 3. Pressure drop Δp and fractional flow f_w of a primary drainage steady-state experiment for cycle 1 (A) and cycle 2 (B) on the same sample (in total, 5 cycles were performed).

In **Figure 5** the raw data of the cycle 1 drainage experiment is displayed in more detail. **Figure 5**A shows the overview of pressure drop Δp, saturation S_w and electrical conductivity as a function of time and injected PV are shown. For selected fractional flows f_w in (B-G) the pressure-drop Δp and saturation S_w are shown with subtracted baseline which provides a more focused visualization of the associated fluctuations. Respective histograms and Fourier spectra of the fluctuations are shown in panels (B-G) in the middle and left.

For fractional flows $f_w > 0.75$ and $f_w = 0.0$ the histograms of the pressure and saturation fluctuations are Gaussian as shown in **Figure 4** and the fluctuation magnitude is more of the order of instrumental noise.

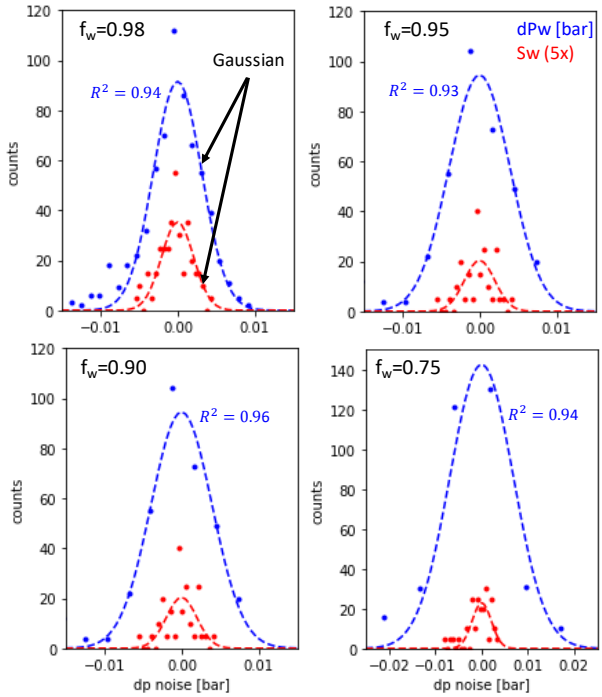

Figure 4. Histograms for Δp and S_w fluctuations (S_w fluctuations are magnified by a factor of 5 for better visibility) from **Figure 5** for $1.0 \geq f_w \geq 0.75$ following a Gaussian behavior (dotted lines are fits with Gaussian).

For $0.67 \geq f_w \geq 0.02$ the fluctuation amplitude is significantly larger than for the other f_w and the histograms are not Gaussian anymore. In many cases the histogram is actually bi-modal (**Figure 5**E,F) and respective pressure and saturation fluctuations are periodic in time with notable peaks in the Fourier spectrum representing the frequency of the periodicity in time. That clearly suggests that the pressure and saturation fluctuations for $0.67 \geq f_w \geq 0.02$ do not represent instrumental noise but have a different cause.

3.2 Separating fluctuations from noise and energy scale

In **Figure 6** pressure and saturation fluctuations are separated from instrumental noise. From the noise statistics for $f_w > 0.75$ where noise amplitudes are consistent with instrumental noise and histograms are Gaussian a noise floor is estimated which is proportional to the respective mean $\overline{\Delta p}$ and $\overline{S_w}$. Pressure fluctuations of up to $\delta\Delta p = 50\ mbar$ are clearly above the thermal noise level. Already for a single pore-filling event the associated pressure-volume work

$$\Delta W_{pressure-volume} = p_c \Delta V \qquad (3)$$

is $\Delta W \approx 4.5 \cdot 10^{-10}\ J$ with $\Delta V \approx 1.1 \cdot 10^{-13} m^3$ for a spherical pore of 60 μm diameter and a capillary pressure $p_c = 2\sigma/r \approx 0.04\ bar$ (for a pore throat of $d = 2r = 25\ \mu m$).

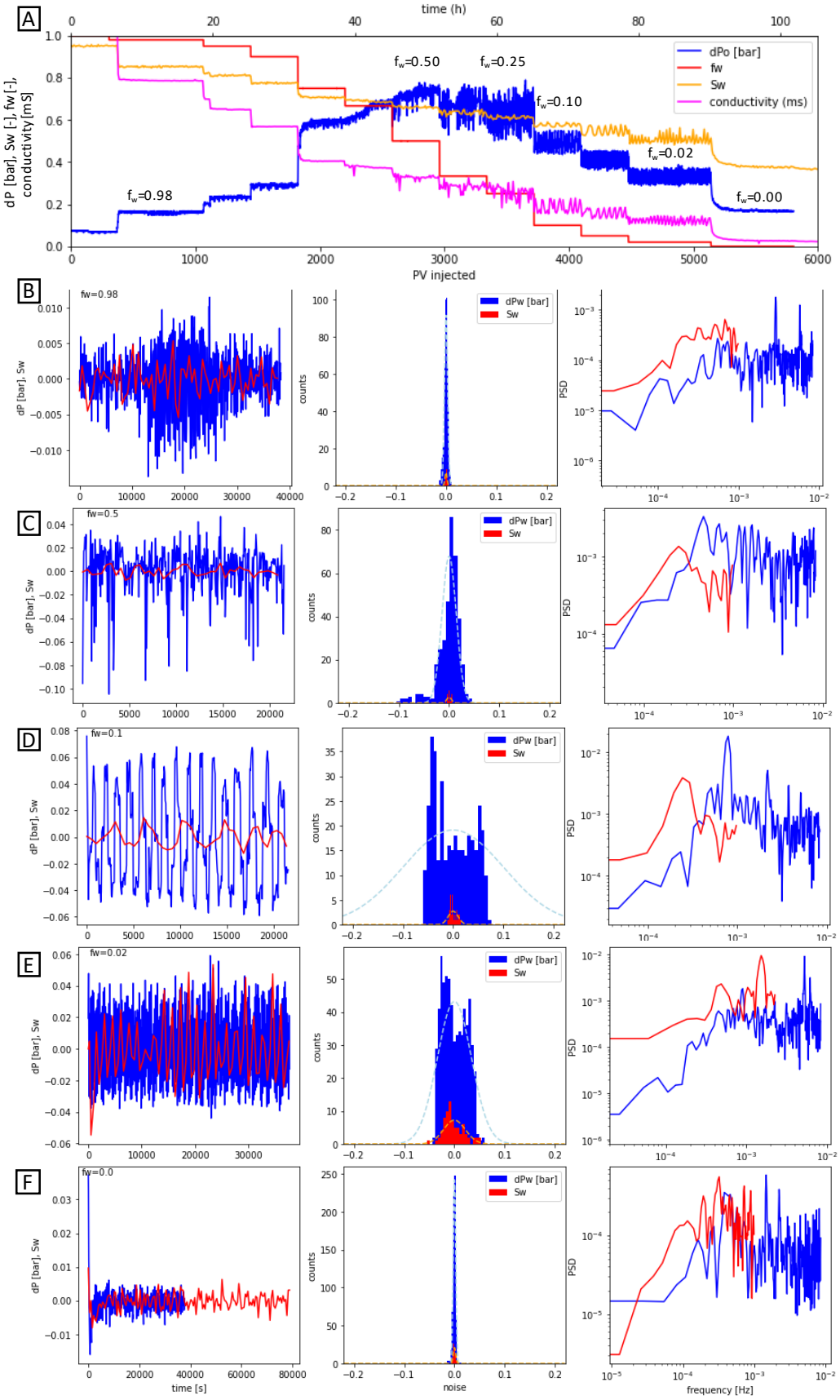

Figure 5. Raw data of the drainage experiment (A) showing pressure drop Δp, saturation S_w and electrical conductivity as a function of time and injected PV. For a number of selected fractional flow f_w (B-G) Δp and S_w are shown with subtracted baseline which provides a clearer focus on the fluctuations (left), the respective histograms for Δp and S_w (middle) and Fourier spectrum (right) of the fluctuations.

Expressed in units of k_BT $\Delta W = 1.1 \cdot 10^{11}\, k_BT$ meaning that pressure fluctuations associated with single pore filling events (Haines jumps) are many orders of magnitude larger than the thermal energy scale. Just as a comparison, pressure-volume work related viscous dissipation from connected pathway flow is of the same order of magnitude as the thermal energy scale.

The saturation fluctuations which can range up to $\delta S_w = \pm 5\%$, however, are much larger than individual pore filling events. For Fontainebleau sandstone with typical pores of volume $V_{pore,single} = 1.1 \cdot 10^{-7}\, cm^3$, 5% fluctuation of saturation for a total pore volume of $V_{pore,tot} = 2.85\, cm^3$ means that a very large number of individual pores are involved.

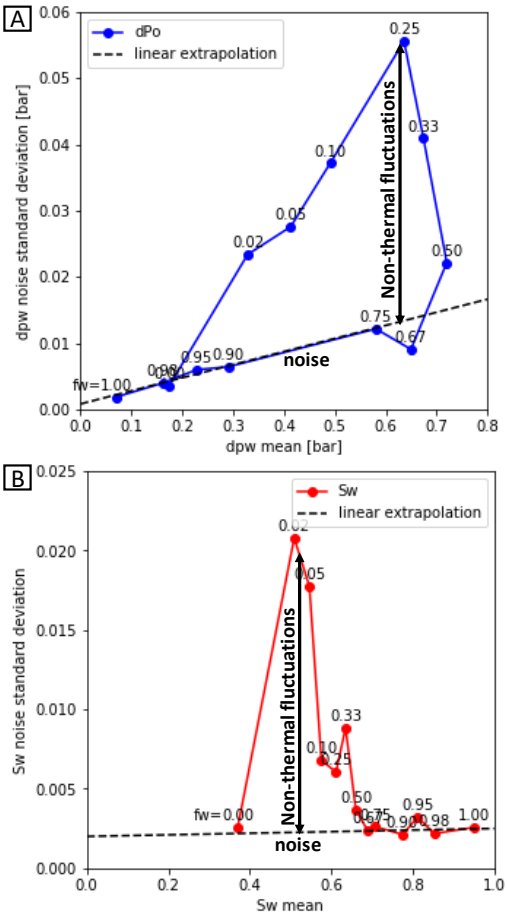

Figure 6. Fluctuations can be separated from instrumental noise by considering the relationship between mean and standard deviation for each f_w. Respective figures for Δp (A) and S_w (B) show a clear deviation from the linear trend for noise (established for $f_w \geq 0.67$) in the range of fractional flows $0.67 > f_w \geq 0.02$. For e.g. $f_w = 0.67$ the fluctuation amplitude is about 3 times larger than the instrumental noise.

3.3 Averaging pressure and saturation raw data

In **Figure 7**A we see that the saturation fluctuations do not follow exactly the same trend as the pressure fluctuations. That can be caused by the different sampling rates of pressure (1 min) and saturation (8min30s) in comparison with the frequency of the fluctuations (**Figure 5**B-G). When averaging or under-sampling the periodic structure of fluctuations can disappear, and fluctuations become Gaussian. That can potentially explain why in **Figure 7** the saturations do not follow exactly the same trend as pressure. It also clearly shows what happens when raw data is averaged or only reported as average to make it "look nicer" because that can hide underlying physics.

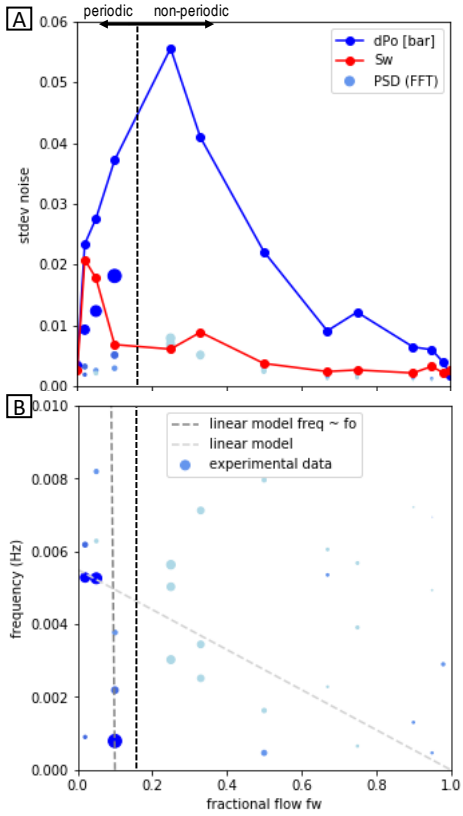

Figure 7. Fluctuation standard deviation as a function of fractional flow (A) shows a systematic trend. Due to the much lower sampling rates it is possible that saturation fluctuations are missed. From the dominant peaks in the Fourier spectrum the fluctuations can be separated into period and non-periodic fractions. The first three dominant peaks in the Fourier transform of the time signal (**Figure 5**B-G, third column) do not scale linearly with injection fractional flow f_w (linear trends - dashed grey lines - do not represent relevant fraction of dominant peaks) (B) .

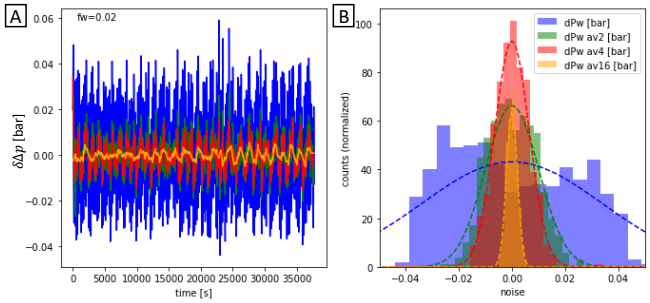

Figure 8. Averaging or under-sampling pressure fluctuations $\delta\Delta p$ (here applying a rolling average over 2, 4 and 16 subsequent samples for $f_w = 0.02$) can hide periodic fluctuations and transform histograms from bimodal to Gaussian (dotted lines) which is ultimately a consequence of the central limit theorem.

3.4 Relative Permeability

From averaged Δp and fluxes the relative permeability can be obtained using the 2-phase Darcy equation (2) but capillary pressure needs to be taken into account e.g. by inverse modelling [1-5,28,29]. In **Figure 9** the relative permeability for all 5 drainage and imbibition cycles are displayed. The 5 cycles superimpose very well with only very little scatter suggesting that the repeatability of the experiment is given. In addition, we show the fractional flow curves (C,F) for the first drainage and imbibition cycle.

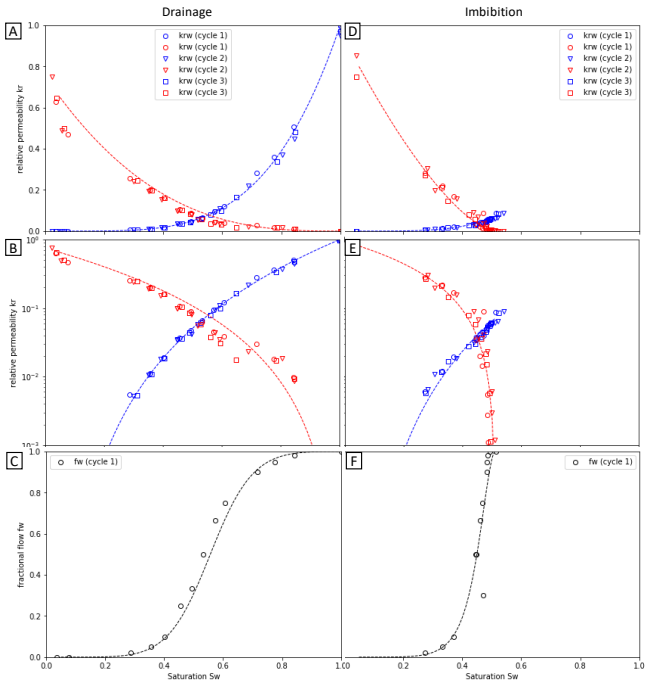

Figure 9. Relative permeability $k_r(S_w)$ for all 5 cycles on a linear (A,D) and logarithmic (B,E) scale, for drainage (A,B) and imbibition (D,E). The dotted line represents a fit with a Corey function. Results for all 5 cycles are very well reproducible. Respective fractional flow curves $f_w(S_w)$ are shown in C,F.

3.5 Travelling Saturation waves

In **Figure 7** the pressure and saturation fluctuations are not only separated from noise but also divided into a mainly periodic and non-periodic fraction. By focusing on the dominant peaks in the Fourier transform of the time signal i.e. power spectral density (PSD) in third column in **Figure 5**B-G we can see **Figure 7**A that the amplitude of the first 3 peaks of $\delta\Delta p$ follows a very similar trend with f_w as the standard deviation. However, as shown in **Figure 7**B the dominant fluctuation frequencies do not linearly scale with fractional flow f_w. That is also an important insight as it rules out simple experimental artefacts such as back pressure regulators or a capillary instability at the injection our outflow [36-38] because these would show a frequency proportional to fractional flow.

The observation that pressure and saturation data time series show systematic but non-linear trends with f_w in general e.g. fluctuations beyond noise level are encountered reproducibly only for $0.67 \geq f_w \geq 0.02$ and highly periodic fluctuations only for $0.20 \geq f_w \geq 0.02$ raises the question even more about the physical origin. When inspecting the saturation profiles $S_w(x)$ for $f_w = 0.10$ and $f_w = 0.05$ where the most periodic fluctuation behavior is observed the saturation profiles $S_w(x,t)$ represented in a space-time contour plot in **Figure 10** show travelling saturation from inlet to outlet in a periodic fashion during the core flooding experiment, even at "steady-state".

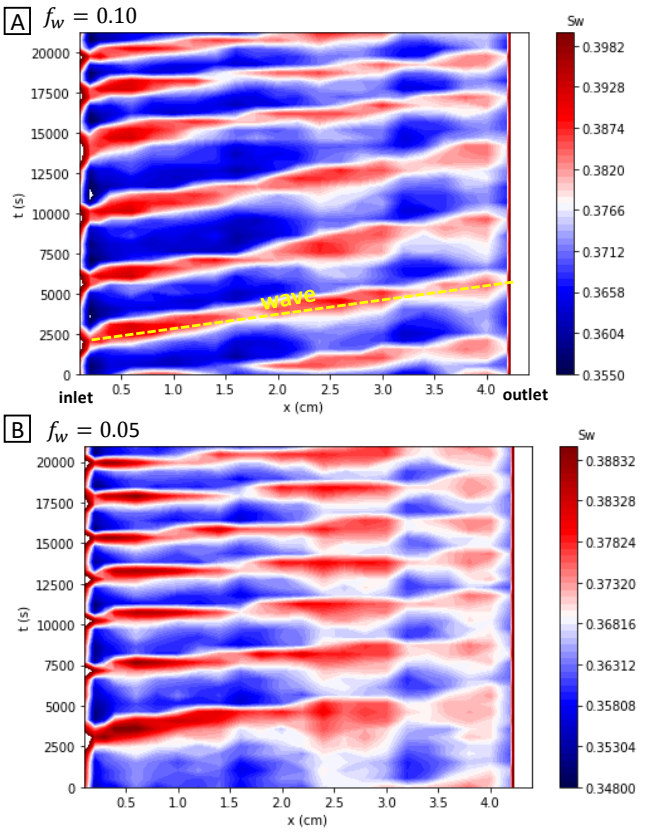

Figure 10. Space-time plot for the saturation $S_w(x,t)$ for $f_w = 0.10$ (A) and $f_w = 0.05$ (B). Travelling saturation waves are visible which travel at nearly constant velocity from inlet to outlet in a periodic manner.

3.6 Fractional flow solution

Saturation profiles consist of a water peak that travels at largely constant velocity from inlet to outlet with an amplitude $\delta S_w \approx 0.04$ consistent with saturation fluctuations in e.g. **Figure 5**F. As already pointed out previously, that saturation change is significant and involves a very large number of individual pores. This suggests that travelling saturation waves are a Darcy scale phenomenon.

Fractional flow theory based travelling wave solutions have been reported in the literature [33,34]. The question is whether that is indeed the situation in our experiment. The validation involves 2 steps: a fractional flow construction for the saturation S_w for the maximum and minimum saturation in the traveling wave solution from **Figure 10**, show for two specific fractional flows at specific times in **Figure 11**.

Starting point for a respective analysis is a hysteresis fractional flow model as shown in **Figure 12** where both drainage and imbibition $f_w(S_w)$ are considered since the moving saturation peak represents water displacing oil

(imbibition) at the leading edge and oil displacing water (drainage) at the trailing edge.

For constructing the fractional flow solution we start with a line from the origin to intersection with the drainage $f_w(S_w)$ at injection fractional flow $f_{w,inj}$ as shown in **Figure 12** [35].

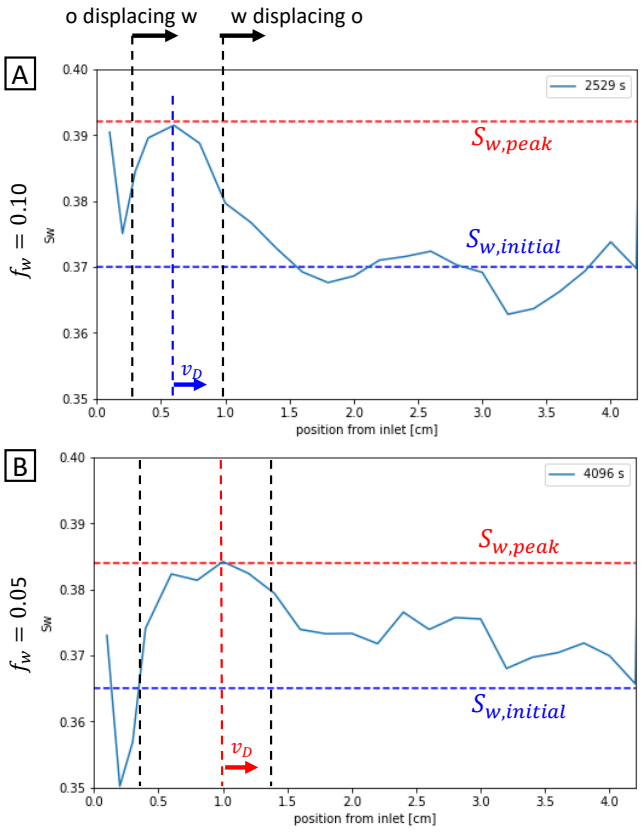

Figure 11. Saturation profiles $S_w(x)$ at a specific time t for $f_w = 0.10$ (A) and $f_w = 0.05$ (B). From an initial water saturation $S_{w,initial}$ a saturation peak $S_{w,peak}$ is observed which moves forward through water displacing oil at the leading edge (imbibition). At the trailing edge, oil displaces water (drainage). In principle both edges can move at different velocities, but the width of the peak in space is less than a capillary dispersion zone [29] and therefore we only operate with an average velocity v_D at which the peak moves and refer to it as an overall drainage process at which the peak is pushed forward by the injected oil fraction.

The fractional flow shock front solution is constructed from imbibition fractional flow $f_{w,im}$ at initial water saturation $S_{w,initial}$ to the intersection of the line (4) and the imbibition $f_{w,im}(S_w)$.

In **Figure 13** this fractional flow construction is applied to the cases for $f_{w,inj} = 0.15$ and $f_{w,inj} = 0.10$. While for $f_{w,inj} = 0.15$ we see a behavior conceptually similar as in the cartoon in **Figure 12** i.e. that the shock front saturation S_w^* which would represent the saturation peak of the travelling wave from **Figure 10** and **Figure 11** is larger than the initial saturation $S_w^* > S_{w,initial}$. However, for fractional flow $f_{w,inj} = 0.10$ we see that $S_w^* < S_{w,initial}$ meaning that there is an inflection point for a fractional flow somewhere $0.07 < f_w^* < 0.12$. For injections above the inflection point $f_{w,inj} > f_w^*$ the shock front saturation increases over the initial saturation i.e. represents an imbibition process, and for $f_{w,inj} < f_w^*$ the shock front saturation decreases i.e. is a drainage process.

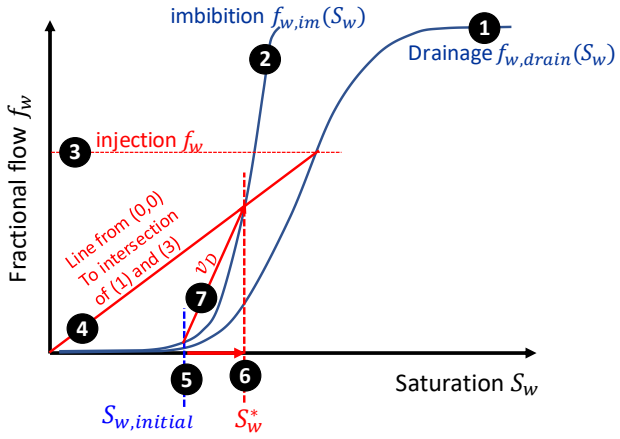

Figure 12. Schematic description of the fractional flow solution for the traveling wave: starting with drainage (1) and imbibition (2) $f_w(S_w)$ curves, a line (4) is drawn from the origin to the intersection (3) of the injection fractional flow $f_{w,inj}$ and the drainage $f_{w,drain}(S_w)$ curve (1). The fractional flow shock front solution (7) is constructed from the imbibition f_w at initial saturation $S_{w,initial}$ (5) to the intersection of line (4) with the imbibition $f_{w,im}(S_w^*)$ at shock front saturation S_w^* (6).

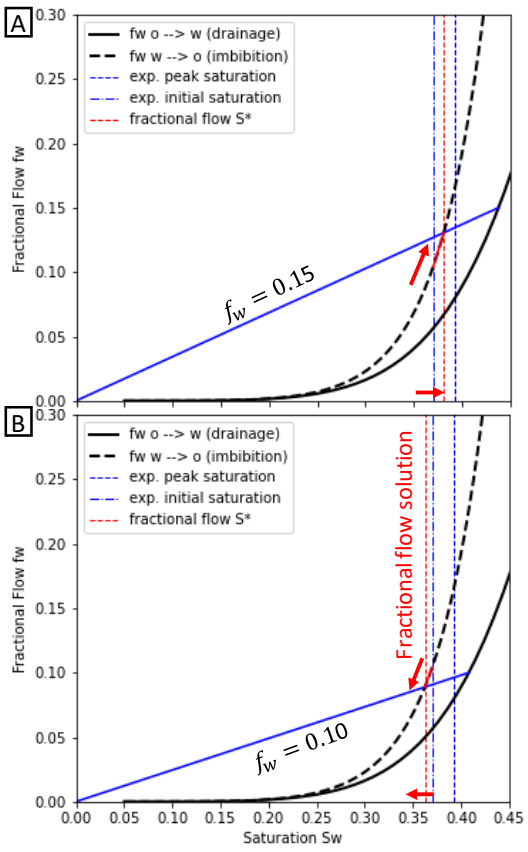

Figure 13. Fractional flow solution for injection at $f_{w,inj} = 0.15$ (A) and $f_{w,inj} = 0.10$ (B) considering the hysteresis fractional flow model from **Figure 12** but with the drainage and imbibition fractional flow curves of the Fontainebleau experiment (**Figure 9**).

Given the limited experimental accuracy and uncertainties with which the initial saturation $S_{w,initial}$ can be determined (see **Figure 11**) which also impacts the fractional flow solution it is very well possible that the $f_{w,inj} = 0.10$ step is still above the inflection point while $f_{w,inj} = 0.05$ would be clearly below the inflection point. From the space-time plot $S_w(x,t)$ in **Figure 10** it is difficult to see any conceptual difference above and below the inflection point f_w^*. Only the slope of the waves in the space-time domain is different which suggest a different propagation speed. However, in the saturation profiles shown in **Figure 11**B we see that for the trailing front the saturation falls below the initial saturation which could indicate that water is pushing oil, i.e. has more of an imbibition character.

3.7 Velocity of the traveling waves

In the next step we compare the propagation velocity of the saturation peak with the prediction from fractional flow theory for the velocity v_D at which saturation S_w propagates

$$v_D|_{S_w} = \frac{x_D}{t_D}\Big|_{S_w} = \frac{df_w}{dS_w}\Big|_{S_w} \qquad (4)$$

where $x_D = x/L$ is the dimensionless distance (L is the length of the core) and $t_D = PV_{injected}/PV$ the dimensionless time expressed in terms of the fraction of injected pore volumes to the pore volume of the core PV.

In the experiment, for $f_{w,inj} = 0.10$ we find $v = 0.76\, mm/min$ which corresponds to a dimensionless velocity $v_D = 0.6$. For $f_{w.inj} = 0.05$ the wave velocity v is between 1.7 and $2.1\, mm/min$ which corresponds to dimensionless velocity $v_D = 2.1 - 2.6$. In **Figure 14** v_D from the two experiments is compared with the fractional flow prediction from eq. 4.

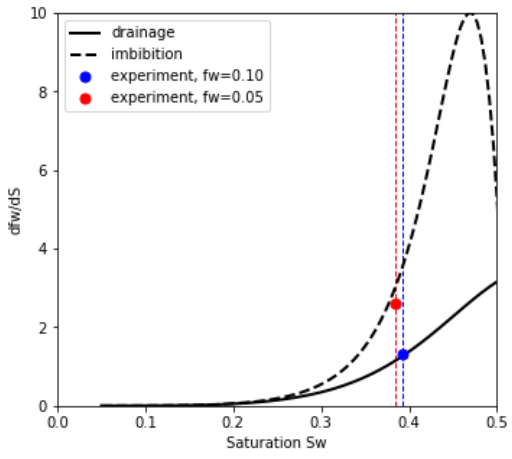

Figure 14. Dimensionless velocity v_D of the propagating saturation peak from **Figure 9** and comparison with the fractional flow prediction where $v_D = df_w/dS_w$ (eq. 4). For injection $f_{w,inj} = 0.10$ we find a behavior compatible with the drainage df_w/dS_w while for $f_{w,inj} = 0.05$ v_D is compatible with imbibition. That is somewhat consistent with the observation of the inflection point somewhere $0.07 < f_w^* < 0.12$ observed in **Figure 13**.

We find that for $f_{w,inj} = 0.10$ the experimental v_D is compatible with a **drainage** behavior consistent with the fractional flow construction above the inflection point i.e. from **Figure 13**A. As already pointed point, even though **Figure 13**B suggests that $f_{w,inj} = 0.10$ is below the inflection point f_w^*, because of the experimental uncertainty it is very well possible that it is actually above the inflection point. v_D being consistent with drainage df_w/dS_w also suggests that overall the velocity of the saturation peak is dominated by the trailing edge.

for $f_{w,inj} = 0.05$ the experimental v_D is compatible with an **imbibition** behavior. That is consistent with the observation that $f_{w,inj} = 0.05$ is clearly below the inflection point f_w^*.

3.8 Physical interpretation of travelling waves

From **Figure 10** it is clear that saturation fluctuations are caused travelling saturation waves. They are also likely the cause of pressure fluctuations as per fractional flow theory, pressure and saturation response are coupled. The observation of different pressure and saturation frequency and amplitudes from **Figure 6** and **Figure 7** can be potentially attributed to the different sampling rates and the associated impact of under-sampling as shown in **Figure 8**.

The remaining question is why we observe travelling waves first place. The traditional expectation is that when a steady-state is reached, saturation is constant in time and space (except for capillary end-effects [29]).

A possible reason for the presence of travelling saturation waves is that for the specific flow conditions, the solution of the governing fractional flow equations are unstable against perturbations such as pore scale displacements, Haines jumps etc. The effects of such instabilities could be shown mathematically by using for instance linear stability analysis.

However, moving banks that are initialized via respective initial conditions do not explain why during constant fractional flow injection the moving saturation banks appear, i.e. why a homogeneous saturation solution becomes unstable against perturbations. In order to prove that, a linear stability analysis of the governing equations e.g. in [33,34] would be required, which would involve a significant level of complexity. Given the degree of uncertainty and assumptions involved it is not clear whether such an analysis can be successful.

Here we follow a different approach and argue more from a physical side why nature would prefer a travelling wave solution over constant saturation. Starting point is the question whether travelling waves would transport more flux than fractional flow at constant saturation. The assessment of that question will be based on the flux $\lambda_\alpha = k_{r,\alpha}/\mu_\alpha$ of phase α. We have to honor the flux boundary condition i.e. injecting water and oil phases at f_w. Therefore, we weigh the mobility of water with f_w and oil with $(1 - f_w)$. For a flat saturation profile we obtain

$$\lambda_{tot}^{flat} = f_w \frac{k_{r,w}^{drain}}{\mu_w} + (1 - f_w)\frac{k_{r,o}^{drain}}{\mu_o} \qquad (5)$$

In order to estimate the total mobility of a travelling saturation wave we treat it as a moving water bank with length $l_w = 0.1 - 0.2$ (i.e. having a length of 10-20% of the total saturation profile, see **Figure 10** and **Figure 11**) and a

saturation height of $\delta S_w = \pm 0.01$ and $\delta S_w = \pm 0.02$. The total mobility of the travelling bank is then

$$\lambda_{tot}^{bank} = l_w \lambda^{water\ bank} + (1 - l_w)\lambda^{oil\ bank} \quad (6)$$

In **Figure 15** we plot the ratio of λ_{bank}^{tot} from eq. 6 over the total mobility of the flat saturation profile λ_{tot}^{flat} from eq. (5), i.e. $\lambda_{bank}^{tot}/\lambda_{tot}^{flat}$. For $\lambda_{bank}^{tot}/\lambda_{tot}^{flat} < 1$ the flat saturation profile has the higher total mobility. But for $\lambda_{bank}^{tot}/\lambda_{tot}^{flat} > 1$ the travelling wave has the total higher mobility. We can see from **Figure 15** that this is the case for saturations $S_w < 0.4 - 0.5$ or $f_w < 0.4$ which is consistent with the general observation

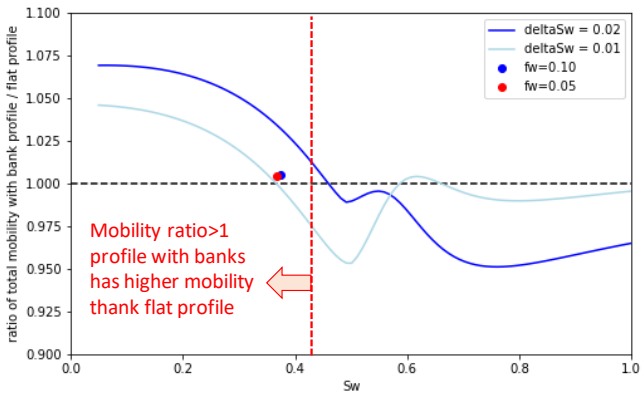

Figure 15. Ratio of the total flux of the travelling saturation waves ("banks") and the total flux of a flat saturation profile. We see that – depending on the saturation wave amplitudes δS_w – the total mobility of the traveling wave solution is higher than for a homogenous saturation profile, meaning that for the same pressure drop more total flux is transported than for a homogenous saturation profile. For a saturation wave amplitude $\delta S_w = \pm 0.01$ that occurs for $S_w < 0.39$ and for $\delta S_w = \pm 0.02$ for $S_w < 0.45$. That is roughly consistent with the experimentally observed onset of fluctuations beyond the noise level from $S_w < 0.4 - 0.5$ or $f_w < 0.4$-0.6.

That means that travelling waves can transport at the same pressure drop more flux than a homogeneous saturation profile, i.e. it is energetically more favorable than transport at a flat saturation profile. Note that this is just a rough approximation and does not replace a more rigorous stability analysis which is subject to future work.

4 Influence of Wettability

In an unrelated study (but with the same experimental setup) we demonstrate the influence of wettability conditions on the magnitude of the pressure and saturation fluctuations. For that study, three cylindrical samples (5 cm length and 3.8 cm diameter) of Bentheimer rock ($\phi = 0.25$, $K = 2.6\ D$, twin-samples taken from the same block specifically selected for homogeneity) were aged with 3 different crude oils (properties listed in **Table 1**) following largely the de-saturation (using a centrifuge) and ageing protocol (40 days) outlined in [41] (but without pre-drilling small sub-samples because these are Darcy scale experiments). The flow experiment was conducted with decalin instead of crude oil.

The raw data for first imbibition experiment for the 3 samples is shown in **Figure 16**A. Based on an extensive analysis of the 3 different crude oils using gas chromatography and cyclotron resonance mass spectrometry methods which allows to distinguish chemical species to the level of functional groups extending significantly beyond TAN, TBN and SARA analysis, the potential for wettability alteration is highest for crude oil 3 followed by crude 2 and the least for crude 1. This is confirmed by the trend of residual oil saturation, $S_{o,r}$ and the water endpoint relative permeability $k_{r,w}(S_{o,r})$ displayed in **Figure 16**B.

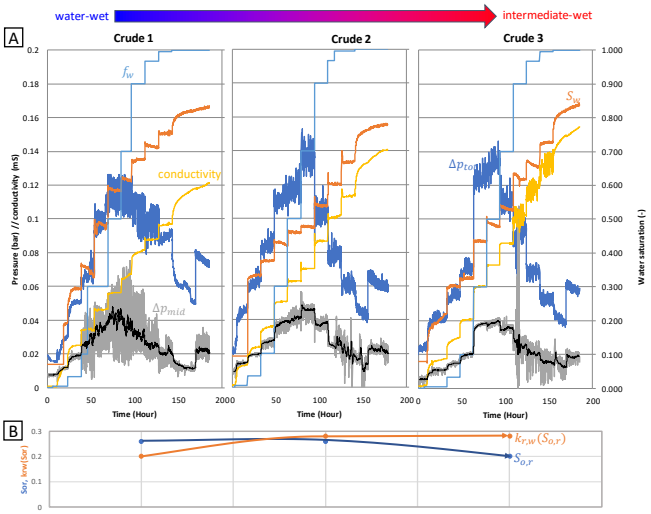

Figure 16. Raw data for 3 steady-state core floods in Bentheimer rock aged with 3 different crude oils (A) resulting in 3 different wettability conditions from more water-wet to more intermediate-wet, consistent magnitude of residual oil saturation, $S_{o,r}$ and water relative permeability endpoint, $k_{r,w}(S_{o,r})$ (B). The magnitude of pressure and saturation fluctuations systematically decreases from water-wet to intermediate-wet conditions.

Table 1. Properties of crude 1, 2 and 3.

Crude	Density	Visc.	TAN	TBN	Sat	Aro	Res
	kg/m^3	mPas	mg KOH/g	mg /kg	wt-%	wt-%	wt-%
1	934.7	88.43	1.37	320	37	48	14
2	833.9	4.87	0.07	83.9	58	37	4
3	859.2	9.47	0.09	271	44	44	10

The pressure and saturation fluctuations shown in **Figure 16**A follow a systematic trend with wettability where the fluctuations are largest for water-wet conditions and lowest for intermediate- to mixed-wet conditions. This observation confirms that that the fluctuations are not an artefact because except for the wettability no other condition was changed and the same setup was used with practically identical rock samples. It rather confirms that the effect is systematically affected by wettability conditions. In an independent set of pore-level experiments conducted with smaller twin-samples

from the same block of Bentheimer rock following the preparation protocol in [41] similar trends i.e. strong fluctuations in the water-wet case [10] and much less fluctuations in the intermediate-wet (aged) case [11] were observed. This confirms, on the one hand, the independent reproducibility of the effect, and on the other hand, links the Darcy-scale observation to pore scale flow regimes. Already a previous study performed in Ketton limestone showed that in mixed-wet rock the flow regimes are systematically different due to enhanced ganglion dynamics [27]. The study by Lin et al. [11] provided the insight of increased connectivity in mixed-wet conditions due to bi-continuous interfaces. Increased connectivity implies less pore scale displacement events together with an overall lower capillary pressure magnitude resulting in lower magnitude of pressure fluctuations. At the same time the different wettability will also impact relative permeability and consequentially the fractional flow curves. A detailed analysis similar to that presented in section (3) would be required to fully understand how that impacts the travelling saturation wave instability.

5 Summary & Conclusions

The raw data of a steady-state (drainage) core flooding experiment in water-wet Fontainebleau sandstone rock shows reproducibly pressure, saturation and electrical conductivity fluctuations in a systematic manner in terms of fractional flow and saturation range but also wettability (for imbibition experiments where rock has been aged with crude). The experimental setup has been designed to rule out common experimental artefacts such as back pressure regulators or complex fluid behavior. Artefacts from e.g. the injection instability (effects in the end-piece and capillary entry pressure for oil) can be also largely ruled out because the effect would be present for all fractional flows and would scale with oil injection rate but that is not what is experimentally observed. In a very recent experiment using the same concepts and in particular the same end pieces as shown in **Figure 2**B the fluid distribution inside the end piece was imaged, observing continuous injection for both oil and water phases. While water injection occurred mainly in the center (and re-distributed in the first few layers of pores) the oil phase is distributed over the whole end face of the core, i.e. no signature of slug-like injection has been observed.

By systematically analyzing the raw data, fluctuations can be separated from instrumental noise suggesting that fluctuations mainly occur in the fractional flow range of $0.67 \geq f_w \geq 0.02$. The saturation space time $S_w(x,t)$ analysis reveals that the underlying reason of saturation (and pressure) fluctuations are travelling saturation waves, which can be reconciled with fractional flow theory. There is also an intuitive physical explanation for traveling saturation waves as a rough estimate reveals that travelling waves transport more flux at the same pressure drop than for flat saturation profiles which occurs roughly in the same fractional flow and saturation range where non-noise fluctuations are observed in the experiment.

That clearly demonstrates that the observation of strong pressure and/or saturation fluctuations in steady-state experiments are not necessarily experimental artefacts or noise but can have a physical origin. This also means that observation of such strong fluctuations can no longer be a reason for dismissing the experiment as invalid. It rather means that we need to update our interpretation methodology for such experiments and this work provides respective guidance.

There are a range of potential consequences which we need to be aware. Travelling saturation waves involve hysteresis because the leading front of a propagating water saturation peak represents an imbibition process while the trailing front is a drainage process. Therefore, construction of the fractional flow solution involves both drainage and imbibition fractional flow curves. That also means that the resulting relative permeability curve measured in such steady-state experiments is not a pure drainage or imbibition bounding curve anymore but rather a scanning curve. Given the complexity of hysteresis models, previous work [34] pointed out that solutions of such models are inherently non-unique. That would explain why interpretation workflows of relative permeability core floods by inverse modelling [1,2] show even with the most flexible relative permeability model still residuals which are non-Gaussian.

The second level of consequences are more conceptual and relate to the transition from pore- to Darcy scale. While we speculate that pore scale events provide a trigger for pressure and saturation fluctuations, it is clear that based on volumetric assessment the saturation change associated with fluctuations involve hundreds to thousands of pores, i.e. are not a pore scale phenomenon anymore. Without a valid fractional flow solution, pore scale fluctuations would eventually average out at REV scale. Only because a valid fractional flow solution exists, they are still visible on the centimeter scale. The length of the moving saturation bank of a few mm is approximately in the same range as the size of the biggest possible oil clusters [39] just before getting mobilized by viscous forces [40] and also approximately the length of a capillary dispersion zone [29]. Therefore, the travelling saturation waves represent the transition from pore to Darcy scale. We have never looked at the transition from pore to Darcy scale in this way which means that it deserves also a more detailed investigation in the future.

Diederik van Batenburg, John van Wunnik and Jasper de Reus are acknowledged for helpful discussions about the fractional flow analysis.

References

1. Berg, S., Unsal, E., Dijk, H., Non-Uniqueness and Uncertainty Quantification of Relative Permeability Measurements by Inverse Modelling, Computers and Geotechnics 132, 103964, 2021.
2. Berg, S., Unsal, E., Dijk, H., Sensitivity and uncertainty analysis for parameterization of multi phase flow models, Transport in Porous Media, *in press,* 2021, DOI: 10.1007/s11242-021-01576-4.
3. Masalmeh, S. K, Sorop, T. G., Suijkerbuijk, B.M.J.M., Vermolen, E.C.M., Douma, S., van der Linde, H. A. and Pieterse, S.G.J. (2014), Low Salinity Flooding: Experimental Evaluation and Numerical Interpretation, IPTC 17558, presented at the International Petroleum

Technology Conference, Doha, Qatar 19-22 January 2014.

4. Sorop, T. G., Masalmeh, S. K., Suijkerbuijk, B. M. J. M., van der Linde, H. A., Mahani, H., Brussee, N. J., Marcelis, F. A. H. M., and Coorn, A. (2015). Relative permeability measurements to quantify the low salinity flooding effect at field scale. In Abu Dhabi International Petroleum Exhibition and Conference held in Abu Dhabi, UAE, 9-12 November 2015, number SPE-177865-MS.
5. Wang, Y., Masalmeh, S.K., Obtaining High Quality SCAL Data: Combining different measurement techniques, saturation monitoring, numerical interpretation and continuous monitoring of experimental data, E3S Web of Conferences 89, 02007, 2019. SCA2018.
6. Clennell, M. B., White, C., Giwelli, A., Myers, M., Esteban, L. Cullingford, M., Richardson, W., Ward, G., Waugh, M., Cole, S., Hunt, A., Bright, P., Improved method for complete gas-brine imbibition relative permeability curves, International Symposium of the Society of Core Analysts held in Pau, France, 26-30 Aug. 2019, paper SCA2019-006.
7. Alcorn, Z. P., Fredriksen, S. B., Sharma, M., Føyen, T., Wergeland, C., Ferno, M. A., Graue, A., Ersland, G., Core-scale sensitivity study of CO_2 foam injection strategies for mobility control, enhanced oil recovery and CO_2 storage, International Symposium of the Society of Core Analysts held in Pau, France, 26-30 Aug. 2019, paper SCA2019-030.
8. Primkulov, B. K., Pahlavan, A. A., Fu, X., Zhao, B., MacMinn, C. W., Juanes, R., Signatures of fluid-fluid displacement in porous media: wettability, patterns and pressures, J. Fluid Mech. 875, R4, 2019.
9. Rücker, M., Berg, S., Armstrong, R. T., Georgiadis, A., Ott, H., Simon, L., Enzmann, F., Kersten, M., de With, S., The Fate of Oil Clusters During Fractional Flow: Trajectories in the Saturation-Capillary Number Space, International Symposium of the Society of Core Analysts held in St. John's Newfoundland and Labrador, Canada, 16-21 August, 2015, paper SCA2015-007.
10. Lin, Q., Bijeljic, B., Pini, R., Blunt, M. J., Krevor, S., Imaging and Measurement of Pore-Scale Interfacial Curvature to Determine Capillary Pressure Simultaneously with Relative Permeability, Water Resources Research 54, 7046-7060, 2018.
11. Lin, Q., Bijeljic, B., Berg, S., Pini, R., Blunt, M. J., Krevor, S. (2019), Minimal surfaces in porous media: Pore-scale imaging of multiphase flow in an altered-wettability Bentheimer Sandstone, Phys.Rev.E 99: 063105.
12. Datta, S. S., Dupin, J.-B., & Weitz, D. A., Fluid breakup during simultaneous two-phase flow through a three-dimensional porous medium. Physics of Fluids, 26, 62004, 2014.
13. Datta, S. S., Ramakrishnan, T. S., & Weitz, D. A., Mobilization of a trapped non-wetting fluid from a three-dimensional porous medium. Physics of Fluids, 26, 22002, 2014.
14. Gao, Y., Lin, Q., Bijeljic, B., Blunt, M. J., X-ray microtomography of intermittency in multiphase flow at steady state using a differential imaging method, 2017.
15. Gao, Y., Raeini, A. Q., Blunt, M. J., Bijeljic, B., Pore occupancy, relative permeability and flow intermittency measurements using X-ray micro-tomography in a complex carbonate, Advances in Water Resources 129, 56-69, 2019.
16. Gao, Y., Lin, Q., Bijeljic, B., Blunt, M. J., Pore-scale dynamics and the multiphase Darcy law, Physical Review Fluids 5 (1), 013801, 2020.
17. Spurin, C., Bultreys, T., Bijeljic, B., Blunt, M. J., Krevor, S., Intermittent fluid connectivity during two-phase flow in a heterogeneous carbonate rock, Physical Review E 100 (4), 043103, 2019.
18. Spurin, C., Bultreys, T., Rücker, M, Garfi, G., Schlepütz, C. M., Novak, V., Berg, S., Blunt, M. J., Krevor, S., Real-time imaging reveals distinct pore scale dynamics during transient and equilibrium subsurface multiphase flow, Water Resources Research 56(12), e2020WR028287, 2020.
19. Armstrong, R.T., Ott, H., Georgiadis, A., Rücker, M., Schwing, A., Berg, S., Sub-second pore scale displacement processes and relaxation dynamics in multiphase flow, Water Resources Research 52(12), 9162–9176, 2014.
20. Reynolds, C.A., Krevor, S., Characterizing flow behavior for gas injection; relative permeability of CO2-brine and N2-water in heterogeneous rocks, Water Resources Research 51, 9464-9489, 2015.
21. Menke, H.P, Gao, Y., Linden, S., Andrew, M.G., Using nano-XRM and high-contrast imaging to inform micro-porosity permeability during Stokes-Brinkman single and two-phase flow simulations on micro-CT images., Advances in Water Resources under review 2021 / Earth ArXiv, https://doi.org/10.31223/osf.io/ubg6p
22. Moebius, F., Or, D., Interfacial jumps and pressure bursts during fluid displacement in interacting regular capillaries, Journal of Colloid and Interface Science 377, 406-415, 2012.
23. DiCarlo DA, Cidoncha JIG, Hickey C (2003) Acoustic measurements of pore scale displacements. Geophys Res Lett 30(17):1901.
24. Reynolds, C. A., Menke, H., Andrew, M., Blunt, M. J., & Krevor, S., Dynamic fluid connectivity during steady-state multiphase flow in a sandstone. Proceedings of the National Academy of Sciences, 114(31), 8187-8192, 2017.
25. Winkler, M., Gjennestad, M. Aa., Bedeaux, D., Kjelstrup, S., Cabriolu, R., Hansen, A., Onsager-Symmetry Obeyed in Athermal Mesoscopic Systems: Two-Phase Flow in Porous Media, Frontiers in Physics 8:60, 2020.
26. Rücker, M., Berg, S., Armstrong, R. T., Georgiadis, A., Ott, H., Schwing, A., Neiteler, R., Brussee, N., Makurat, A., Leu, L., Wolf, M., Khan, F., Enzmann, F., Kersten, M., From Connected Pathway Flow to Ganglion

Dynamics, Geophysical Research Letters 42, 3888-3894, 2015.

27. Rücker, M., Bartels, W.-B., Singh, K., Brussee, N., Coorn, A., van der Linde, H., Bonnin, A., Ott, H., Hassanizadeh, S.M., Blunt, M.J., Mahani, H., Georgiadis, A., Berg, S., The Effect of Mixed Wettability on Pore Scale Flow Regimes Based on a Flooding Experiment in Ketton Limestone, Geophysical Research Letters 46(6), 3225-3234, 2019.
28. Kokkedee J.A., Boom W., Frens A.M., Maas J.G., Improved special core analysis: scope for a reduced residual oil saturation, Proceedings of Society of Core Analysis conference paper 9601, 1-13, 1996.
29. Huang, D. D. and Honarpour, M. M., Capillary end effects in coreflood calculations, Journal of Petroleum Science and Engineering 19: 103-117, 1998.
30. Berg, S., Rücker, M., Ott, H., Georgiadis, A., Van der Linde, H., Enzmann, F., Kersten, M., de With, S., Becker, J., Wiegmann, A., Connected pathway relative permeability from pore-scale imaging of imbibition. Advances in Water Resources, 90, 24-35, 2016.
31. Jacquin, C., Correlations between the permeability and the geometric characteristics of the Fontainebleau gres. Rev. Inst. Fr. Pet. 19: 921- 937, 1964.
32. Al Saadi, F., Wolf, K., Kruijsdijk, C. V. Characterization of Fontainebleau sandstone: Quartz overgrowth and its impact on pore-throat framework. Journal of Petroleum & Environmental Biotechnology, 7(328), 1-12, 2017.
33. Plohr, B., Marchesin, D., Bedrikovetsky, P., Krause, P., Modeling hysteresis in porous media flow via relaxation, Computational Geosciences 5, 225-256, 2001.
34. Corli, A., Fan, H., Two-phase flow in porous media with hysteresis, Journal of Differential Equations 265, 1156-1190, 2018.
35. Lake, L. W., Enhanced Oil Recovery, Prentice Hall, 1984.
36. Unsal, E., Mason, G., Morrow, N.R., Ruth, D.W., Co-current and counter-current imbibition in independent tubes of non-axisymmetric geometry, Journal of colloid and interface science 306 (1), 105-117, 2007.
37. Unsal, E., Mason, G., Ruth, D.W., Morrow, N.R., Co- and counter-current spontaneous imbibition into groups of capillary tubes with lateral connections permitting cross-flow, Journal of colloid and interface science 315 (1), 200-209, 2007.
38. Unsal, E., Mason, G., Morrow, N.R., Ruth, D.W., Bubble snap-off and capillary-back pressure during counter-current spontaneous imbibition into model pores, Langmuir 25 (6), 3387-3395, 2009.
39. Georgiadis, A., Berg, S., Maitland, G., Makurat, A., Ott, H., Pore-Scale micro-CT Imaging: Non-Wetting Phase Cluster Size Distribution During Drainage and Imbibition, Physical Review E 88(3), 033002, 2013.
40. Armstrong, R. T., Georgiadis, A., Ott, H., Klemin, D., Berg, S., Pore-scale mobilization of non-wetting phase ganglia and critical capillary number for onset of macroscopic capillary desaturation, Geophys. Res. Lett., 41, 1-6, 2014.
41. Lin, Q., Bijeljic, B., Krevor, S.C., Blunt, M.J., Rücker, M., Berg, S., Coorn, A., van der Linde, H., Georgiadis, A., Wilson, O.B., A new waterflood initialization protocol for pore-scale multiphase flow experiments, Petrophysics 60(02), 264-272, 2019.